# Raman spectroscopic study of artificially twisted and non-twisted trilayer graphene

Cite as: Appl. Phys. Lett. **118**, 133101 (2021); https://doi.org/10.1063/5.0040716
Submitted: 15 December 2020 . Accepted: 08 March 2021 . Published Online: 30 March 2021

Sanghyun Kim, Donghyeon Lee, Binbin Wang, Shang-Jie Yu, Kenji Watanabe, Takashi Taniguchi, Jonathan A. Fan, Jiamin Xue, and Kayoung Lee

Applied Physics Letters ARTICLE scitation.org/journal/apl

# Raman spectroscopic study of artificially twisted and non-twisted trilayer graphene

Cite as: Appl. Phys. Lett. **118**, 133101 (2021); doi: 10.1063/5.0040716
Submitted: 15 December 2020 · Accepted: 8 March 2021 ·
Published Online: 30 March 2021



Sanghyun Kim,[1] Donghyeon Lee,[1] Binbin Wang,[2] Shang-Jie Yu,[3] Kenji Watanabe,[4] Takashi Taniguchi,[5] Jonathan A. Fan,[3] Jiamin Xue,[2] and Kayoung Lee[1,6,a)]

## AFFILIATIONS

[1]School of Materials Science and Engineering, Gwangju Institute of Science and Technology (GIST), 123 Cheomdangwagi-ro, Buk-gu, Gwangju 61005, South Korea
[2]School of Physical Science and Technology, ShanghaiTech University, Shanghai 201210, China
[3]Department of Electrical Engineering, Stanford University, Stanford, California 94305, USA
[4]Research Center for Functional Materials, National Institute for Materials Science, 1-1 Namiki, Tsukuba 305-0044, Japan
[5]International Center for Materials Nanoarchitectonics, National Institute for Materials Science, 1-1 Namiki, Tsukuba 305-0044, Japan
[6]School of Electrical Engineering, Korea Advanced Institute of Science and Technology (KAIST), 291 Daehak-ro, Yuseong-gu, Daejeon 34141, South Korea

[a)]**Author to whom correspondence should be addressed:** kayoung.lee@kaist.ac.kr

## ABSTRACT

Twisted van der Waals systems have been receiving recent attention due to their potential for moiré-induced band modulation and corresponding exotic correlated phases. Here, we present a Raman spectroscopic study of artificial trilayer graphene (3LG), represented by monolayer graphene (1LG) on top of Bernal-stacked bilayer graphene (2LG), as a function of the twist angle ($\theta_t$) with respect to each other. The artificially twisted 3LG with $\theta_t > 5°$ shows a distinctive 2D peak, which is literally composed of the typical 2D peak of 1LG and that of 2LG, without signatures of strong coupling between the 1LG and the 2LG. The overall trends of the relative Raman shift and the full width at half maxima of the 2D peak are also provided as a function of $\theta_t$ ranging from 0° to 30°. In particular, non-twisted 3LG shows 2D peak characteristics very similar to those of natural Bernal-stacked 3LG, revealing that the top 1LG and the bottom 2LG are translationally rearranged to be the most thermodynamically stable state. We also realized slightly twisted 3LG with a finite $\theta_t < 1°$, which presents the signature of coexisting Bernal-stacked (ABA) and rhombohedral (ABC) 3LG domains.



Positioning one two-dimensional atomic crystal above another with a relative twist angle ($\theta_t$) between them destroys the translational symmetry of each layer and can create unprecedented moiré superlattices, giving rise to a wealth of exotic phenomena.[1–5] For instance, twisted bilayer graphene (2LG) with $\theta_t$ of near 1.1° presents unconventional superconductivity and strongly correlated insulating phases.[6,7] In addition, rhombohedral (ABC) trilayer graphene (3LG) on rotationally aligned hexagonal boron nitride (hBN)[8,9] and twisted double 2LG[10,11] has shown electrically tunable correlation phenomena associated with van Hove singularities and low-energy flat bands. Twisted 3LG comprising monolayer graphene (1LG) and Bernal-stacked 2LG (AB 2LG) with a finite $\theta_t$ has been realized recently, producing a variety of correlated and topological phases that are highly tunable as a function of $\theta_t$ and an electric field.[12,13]

In this Letter, we investigate the Raman characteristics of artificially twisted and non-twisted 3LG, 1LG stacked on top of AB 2LG with zero or a finite $\theta_t$ on a bottom hBN dielectric (1LG/2LG/hBN). Raman spectroscopy is a powerful non-invasive tool that allows us to explore the electronic and vibrational properties of carbon-based materials.[14–16] In particular, the behavior of 2D Raman peaks in graphene-based systems originating from a double-resonant process provides rich information, such as doping,[17,18] strain,[19–21] and the number of layers.[22,23] Despite existing reports on Raman characteristics of twisted 2LG,[24–26] Raman studies on twisted multilayer graphene with more than two graphene layers are rare.[27] Here, we provide a systematic study on the Raman characteristics of artificially made twisted and non-twisted 3LG as a function of $\theta_t$ ranging from 0° to 30°. Our artificial 3LG with $\theta_t \sim 0°$ shows Raman properties similar to those of natural Bernal-stacked 3LG (ABA 3LG) in terms of the full width at half maximum (FWHM), position, and shape of the 2D peak spectrum. The 2D peak of the slightly twisted 3LG (with a finite $\theta_t < 1°$) reveals the signature of coexisting ABA and ABC 3LG domains.

Our twisted and non-twisted 3LG were fabricated using the "tear-and-stack" dry-transfer technique[28] with an exfoliated graphene flake containing 1LG and 2LG, allowing a precise rotational alignment between 1LG and 2LG (Fig. S1 in the supplementary material).[12] Artificial 3LG was also prepared based on straight edges of separately exfoliated 2LG and 1LG flakes; straight edges of exfoliated graphene generally indicate arm-chair or zig-zag edges.[29] Based on the straight edges of 2LG and 1LG, the rotational alignment between them is realized by rotating the supporting stage of 1LG by a desired $\theta_t$ before picking up the 1LG with 2LG. Using these methodologies, we realized twisted 3LG (Figs. 1 and 2) and non-twisted 3LG (Fig. 3).

While the tear-and-stack method provides delicate twist-control, we admit that unintentional errors in the twist-control can occur when separate 2LG and 1LG flakes are stacked based on their seemingly straight edges. $\theta_t$ was confirmed based on the R or R′ Raman peak position, which is further discussed below. Most of our 1LG/2LG/hBN samples were annealed at 400 °C for 1 h in flowing $H_2$/Ar gas (50 ml/min), unless otherwise stated. For a few samples with a finite $\theta_t < 1°$, Raman spectroscopic characteristics obtained before and after annealing were compared. Raman spectra were obtained using a Micro-Raman Spectroscopy System with a ×100 microscope objective. An excitation laser wavelength of 514 nm and double-edge filters cutting at ∼120 $cm^{-1}$ were used. To avoid laser-induced heating in samples, the laser power was maintained at ∼3 mW. Spatial Raman maps of 2D peak FWHM were constructed using the FWHM value of a single Lorentzian fitted to each 2D peak, which allows differentiation between ABA and ABC 3LG.[30,31]

Figure 1(a) shows an optical micrograph of sample T1, one of our twisted 3LG, where the edges of 2LG and 1LG flakes are marked as red and yellow dashed lines, respectively. Figure 1(b) is the atomic force microscope image showing the overlapped 3LG region of T1; while a few bubbles and wrinkles were made during the transfer process, several notable $\mu$m-range bubble-free and residue-free areas are visible. A small but consistently measured Raman peak at around ∼1470 $cm^{-1}$, which is the R peak,[26] can be seen in Fig. 1(c). The R and R′ Raman peaks originate from the rotation-induced superlattice,[24,26] which was used to confirm $\theta_t$. Figure S2 in the supplementary material provides the Raman spectra of our multiple samples with R or R′ peaks. Based on the position of the R peak, the $\theta_t$ between the 2LG and the 1LG crystal lattices was estimated as ∼14°.[26,27] Figure 1(d) shows that the 2D peak of sample T1 is composed of the 2D peaks of 1LG and 2LG, analysis as performed for 1LG stacked on 3LG with a finite $\theta_t$;[27] the 2D peaks of 1LG and 2LG in Fig. 1(d) were obtained from the non-overlapping 1LG and 2LG regions of sample T1 on hBN. This signifies that the 2D peak of sample T1 can be explained mainly by 2D-peak-related double resonance (Raman scattering) processes separately occurring in each 1LG and 2LG.[32] This also suggests that the interlayer interaction between the top 1LG and bottom 2LG is weak, and interaction-induced band reconstruction is negligible. This is because the energy bands of the top 1LG and bottom 2LG are not rotationally aligned, and interlayer coupling between the two layers is relatively small.[27] The 2D peak of the 1LG was blueshifted by ∼12.9 $cm^{-1}$ to fit to the 2D peak of T1, revealing reduced Fermi velocity caused by a small but existing interlayer coupling potential between the 1LG and 2LG.[33] Figure 1(e) shows that the 2D peak FWHM values are homogeneous as ∼42.4 ± 0.4 $cm^{-1}$ within the overlapped 3LG region.

Figure 2(a) shows the 2D Raman peak profile of our artificial 3LG with different $\theta_t$ (ranging from 0° to 30°). We also provide the Raman spectra of our multiple samples with different $\theta_t$ in a wider Raman shift range, normalized to the G peak of each spectrum, accompanied by the normalized 2D peak intensity vs $\theta_t$, in Fig. S3 in the supplementary material. The 2D peak positions of natural 1LG and our artificial 3LGs with $\theta_t > 5°$ are marked for comparison. The 2D peaks of all artificial 3LGs are blueshifted relative to the 2D peak of 1LG by the reduced Fermi velocity,[33] and the blueshift is strongly $\theta_t$-dependent, as displayed in Fig. 2(b). The overall $\theta_t$-dependence of the peak position is comparable to that of twisted 2LG,[25] governed by the weak but existing interaction between the 1LG and 2LG (i.e., band renormalization). The Raman characteristics of our non-twisted 3LG with $\theta_t = 0°$ [see Fig. 2(a), black line] are surprisingly similar to those of natural ABA 3LG, which are further discussed in Fig. 3. The blueshift decreases from 18.87 $cm^{-1}$ at $\theta_t = 0°$ to 3.91 $cm^{-1}$ at $\theta_t = \sim 5.5°$ before increasing sharply at $\theta_t = \sim 11°$; the 2D peak position change is not monotonic. As $\theta_t$ increases, the 2D peak blueshift approaches a finite value of ∼8 $cm^{-1}$, similar to previous observations of twisted 2LG.[25] Figure 2(c) shows the 2D peak FWHM values of our artificial 3LG as a function of $\theta_t$. As seen in Fig. 1(d), the 2D peak of artificial 3LG with $\theta_t > 5°$ is explained as the overlap of 2D peaks from 1LG and 2LG, and the FWHM values are relatively smaller than that of natural ABA or ABC 3LG, which has more paths for the double

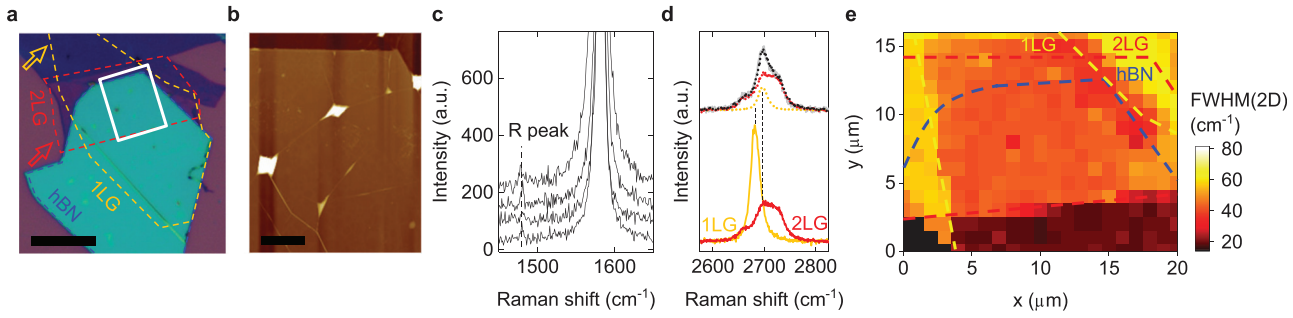


**FIG. 1.** (a) Optical micrograph and (b) atomic force microscope image of sample T1. The scale bars in (a) and (b) denote 10 $\mu$m and 2 $\mu$m, respectively. (c) Consistent R peaks shown in the spectra obtained from multiple points in the overlapped 3LG region of T1. (d) Superposition of the 2D peak spectra of the constituent 1LG (yellow line) and 2LG (red line), producing a spectrum (black dots) akin to the 2D peak of the twisted 3LG (gray line). (e) Raman map of the 2D peak FWHM of T1. The edges of the 1LG, 2LG, and hBN are denoted as yellow, red, and blue dashed lines, respectively.

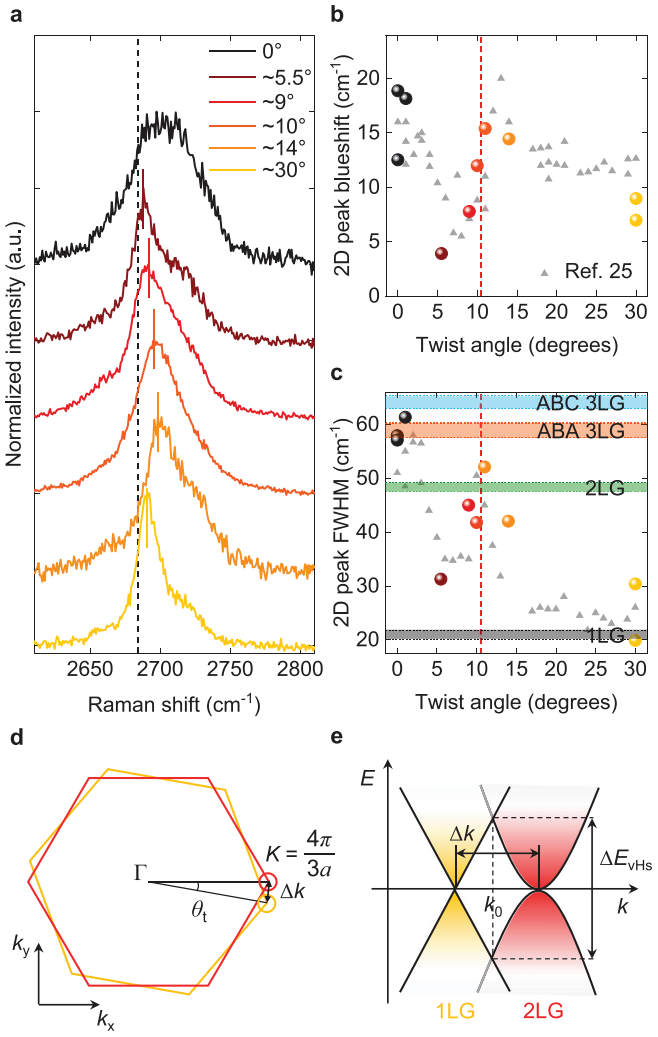


**FIG. 2.** (a) 2D peak spectra of our artificial 3LG with different $\theta_t$. The position of the 2D peak of natural 1LG is denoted as a dashed line. (b) 2D peak blueshift relative to that of natural 1LG and (c) the FWHM as a function of $\theta_t$. The 2D peak blueshift and FWHM values of twisted 2LG were adapted (gray triangles) for comparison.[25] (d) Brillouin zone of twisted 3LG consisting of 1LG and 2LG. The yellow and red circles represent the Fermi contours of the 1LG and 2LG, respectively. The distance between the two nearest K points of the 1LG and 2LG is represented as $\Delta k$. (e) Low-energy bands of the 1LG (yellow) and 2LG (red) overlapping each other.

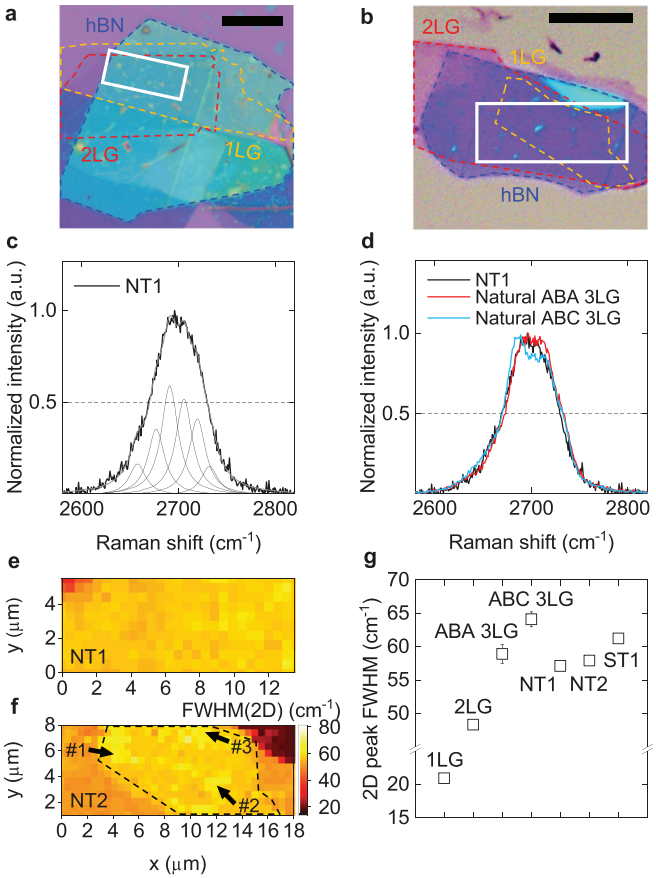


**FIG. 3.** Optical micrographs of (a) NT1 and (b) NT2. The scale bars in (a) and (b) denote 10 $\mu$m, with the edges of hBN, 2LG, and 1LG being marked as blue, red, and yellow dashed lines, respectively. (c) The 2D peak of NT1, which is fitted with six Lorentzian peaks (peak width = 21 cm$^{-1}$) conventionally used to fit to the 2D peak of natural 3LG.[31,38] (d) Direct comparison of the 2D peaks for NT1, natural ABA, and ABC 3LG. (e) and (f) Raman maps of the 2D peak FWHM for NT1 and NT2, obtained from the rectangular regions marked in (a) and (b), respectively. (g) 2D peak FWHM values of natural 1LG, AB 2LG, ABA 3LG, and ABC 3LG compared to those of our artificial 3LG samples (NT1, NT2, and ST1). The error bars represent 95% confidence intervals. Note that the points without error bars have 95% confidence intervals smaller than the size of the symbol.

resonance.[30] It is noteworthy that both 2D peak blueshift and FWHM show sharp increases at $\theta_t = \sim 11°$.

We explain these sharp increases in the 2D peak blueshift and FWHM at $\theta_t = \sim 11°$ based on the simply overlapped low-energy bands[25] of 1LG and 2LG; additional band reconstruction due to weak interlayer interaction between the 1LG and 2LG is ignored. Figure 2(d) describes the first Brillouin zones of 1LG (yellow hexagon) and 2LG (red hexagon) with a finite $\theta_t$, and Fig. 2(e) describes the overlapped low-energy bands of 1LG and 2LG. We neglect the detailed band reconstruction near the region where the energy bands of the 1LG and 2LG overlap. The energy between the two van Hove singularity points ($\Delta E_{vHs}$), where the two low-energy bands overlap each other [Fig. 2(e)], corresponds to

$$\Delta E_{vHs} = 2\hbar k_0 v_f = \hbar^2 (\Delta k - k_0)^2 / m^*, \quad (1)$$

where $m^* = 0.054\, m_e$ is the electron effective mass in 2LG,[34] $v_f = 10^6$ m/s is the Fermi velocity of 1LG,[35] $\hbar$ is the reduced Planck constant, $k_0$ is the wavevector at the van Hove singularity point relative to the nearest K point of the 1LG, and $\Delta k$ is the distance between the two K points of the overlapping 1LG and 2LG [Fig. 2(e)]. This provides $\Delta k$ as a function of $\Delta E_{vHs}$,

$$\Delta k = 0.5\left(\Delta E_{vHs} + 2v_f (m^* \Delta E_{vHs})^{1/2}\right)/\hbar v_f. \quad (2)$$

The relation between $\theta_t$ and $\Delta E_{vHs}$ for twisted 3LG is then written as

$$\theta_t = \Delta k/K = 0.5(3a/4\pi)\left(\Delta E_{vHs} + 2\upsilon_f(m^*\Delta E_{vHs})^{1/2}\right)/\hbar\upsilon_f, \quad (3)$$

where $a = 2.46$ Å is the lattice constant of graphene.[36] For the Raman excitation energy $E_{laser} = 2.4$ eV, which we used for the Raman spectroscopy, Eq. (3) yields the critical twist angle $\theta_c = 10.5°$, at which $E_{laser} \approx \Delta E_{vHs}$; this is marked by red dashed lines in Figs. 2(b) and 2(c). Interestingly, $\theta_c = 10.5°$ agrees very well with the $\theta_t$, at which the sharp increases in both 2D peak blueshift and FWHM were experimentally observed [Figs. 2(b) and 2(c)]. This is because of the dramatically increased density of states and the correspondingly decreased Fermi velocity near the van Hove singularity points, where the two energy bands overlap [Fig. 2(e)].[37]

Figures 3(a) and 3(b) show optical micrographs of non-twisted 3LG samples NT1 and NT2, respectively. Figure 3(c) shows a 2D peak spectrum of NT1 accompanied by six Lorentzians with a fixed FWHM of 21 $cm^{-1}$ fitted to the spectrum. In contrast to the twisted 3LG with $\theta_t > 5°$, the 2D peak spectrum of the non-twisted 3LG is very similar to that of natural ABA 3LG [Fig. 3(d)]. AB 2LG can be formed by stacking two 1LG flakes with a rotational alignment.[28] In contrast to the sole commensurate state for 2LG (AB 2LG), there are two commensurate states for 3LG: ABA and ABC 3LG.[39] We mechanically stacked 1LG on top of 2LG with a rotational alignment, but the translational alignment cannot be atomically controlled in the macroscopic stacking process. Our non-twisted 3LG was then annealed, allowing for thermal activation of the stacking transition from a random incommensurate stacking to ABA-stacking order, which is energetically more favorable than ABC-stacking as well as any other incommensurate 3LG states. Figures 3(e) and 3(f) show 2D peak FWHM maps of NT1 and NT2, respectively, with associated average FWHM values of 57.1 $cm^{-1}$ and 57.9 $cm^{-1}$. These values are in good agreement with that of ABA 3LG [Fig. 3(g)], suggesting the formation of ABA 3LG. Figure 3(g) compares the 2D peak FWHM values of our non-twisted artificial and natural 3LG. The 2D peak FWHM values of our artificial non-twisted 3LG are relatively uniform over the entire region [Figs. 3(e)–3(g)]. There is a limited precision in the $\theta_t$-control, allowing even a single sample to experience slight $\theta_t$ variance due to existing wrinkles and bubbles that add local strain. For instance, NT1 and NT2 exhibit ABA-like spectra, in general, over the overlapped 3LG region but show ABC-like spectra (Fig. S4 in the supplementary material) locally near bubbles, marked by arrows in Fig. 3(f).

In addition, Fig. S5 in the supplementary material shows the influence of the substrate on the 2D peak position and FWHM. While the FWHM does not show much dependence, the 2D peak position varies noticeably depending on the presence of bottom hBN. The natural ABA 3LG and NT1 both manifest relative blueshifts of the 2D peaks when they placed on hBN/$SiO_2$/Si, compared to being placed on $SiO_2$/Si. The 2D peak blueshift is due to enhanced screening by the dielectric substrate[40] as well as the hBN-induced phonon and electronic band modification.[41] In particular, we note that the 2D peak position and FWHM values of NT1 on hBN are very analogous to those of natural ABA 3LG, while those of NT1 on $SiO_2$ largely differ from those of natural ABA 3LG. This indicates that hBN substrates are more favorable to fabricate ABA 3LG, close to its natural state, thanks to the negligible environmental effect of hBN.[41]

Figure 4(a) shows the Raman 2D peak spectrum of slightly twisted 3LG (a finite $\theta_t < 1°$) (sample ST1) obtained before annealing (black line). The 2D peak seems similar to that of ABA 3LG (red line),

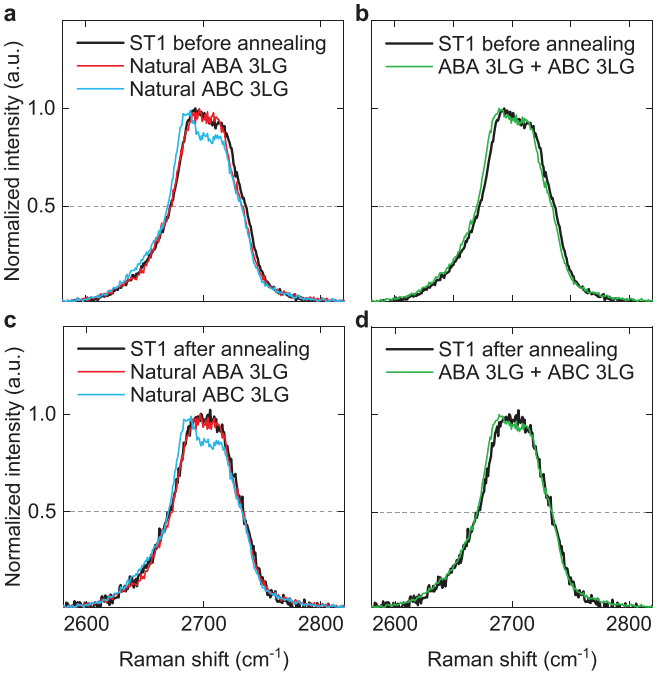


**FIG. 4.** (a) and (b) Raman 2D peak of slightly twisted 3LG (ST1) obtained before annealing. The spectrum is compared to those of natural ABA (red) and ABC (blue) 3LG in (a) and to the sum of the spectra for natural ABA and ABC 3LG in (b). (c) and (d) Raman 2D peak of ST1 obtained after annealing. The spectrum is compared to those of natural ABA (red) and ABC (blue) 3LG in (c) and to the sum of the spectra for natural ABA and ABC 3LG in (d).

but an asymmetric peak characteristic is noticeable, similar to that of ABC 3LG (blue line). We note that the spectrum of ST1 is more similar to the sum of 2D peaks for natural ABA and ABC 3LG [green line in Fig. 4(b)], suggesting the existence of both ABA- and ABC-stacking domains. If 1LG is stacked on top of AB 2LG with a small $\theta_t$, the stacking order will gradually vary from ABA to ABB and then to ABC, assuming each graphene layer is rigid. In reality, atomic reconstruction can happen based on the competition between the interlayer interaction energy and the elastic energy;[42,43] by overcoming small elastic energy, the stacking order can change to the commensurate state, ABA or ABC-stacking, which has a smaller interaction energy. ABA or ABC-stacking (commensurate) domains broaden as much as possible, which are distinctly separated by fine incommensurate stacking boundaries in slightly twisted 3LG.[42–44] The Raman spectrum of ST1 obtained before annealing, which is akin to the sum of 2D peaks for natural ABA and ABC 3LG, reveals the existence of both ABA- and ABC-stacking domains. ABA- and ABC-stacking domains, smaller than the spot size of the laser used in our Raman measurements, may lead to the 2D peak constructed by the mixture of 2D peaks for both ABA and ABC 3LG [Fig. 4(b)]. The Raman spectrum of ST1 obtained after annealing, by contrast, is clearly symmetric and more similar to that of ABA 3LG rather than the sum of 2D peaks for ABA and ABC 3LG [Figs. 4(c) and 4(d)]. This suggests that the thermal energy allows the top 1LG and the bottom 2LG to rearrange to be the most thermodynamically stable ABA-stacked 3LG, similar to the formation of AB-stacked 2LG by stacking two 1LG flakes with a small $\theta_t < 5°$ and

successive annealing.[45] Figure S6 in the supplementary material shows the scanning tunneling microscopy (STM) image of slighted twisted 3LG (a finite $\theta_t < 1°$) after annealing. The topography further confirms the uniformity and the formation of hexagonal lattice without moiré pattern.

In summary, we report Raman characteristics of artificial twisted and non-twisted 3LG (1LG on top of AB 2LG) with various $\theta_t$. The overall trends of the relative Raman shift and the FWHM of the 2D peak are provided as a function of $\theta_t$ ranging from 0° to 30°. The sharp increases in the 2D peak FWHM and the blueshift are observed in the twisted 3LG with $\theta_t \sim 10.5°$, at which incident laser energy equals the energy difference between the two van Hove singularity points ($E_{laser} \approx \Delta E_{vHs}$). Our non-twisted 3LG shows a 2D peak akin to that of natural ABA 3LG. The Raman signature of slightly twisted 3LG (with a finite $\theta_t < 1°$), by contrast, reveals the existence of both ABA- and ABC-stacking 3LG domains.

Twistronics has recently emerged as a state of the art approach to tailor the properties of two-dimensional materials by controlling the relative $\theta_t$ between layers.[12,13,46–49] For twistronic applications, an accurate control of the $\theta_t$ and identifying the precise $\theta_t$ are crucial. Atomic scale imaging tools such as transmission electron microscopy or STM have been mainly employed to determine the $\theta_t$,[42,50,51] which are certainly powerful tools. However, those are time-consuming and not accessible for many researchers. Indeed, Raman spectroscopy is advantageous for quick as well as delicate characterization of graphene-based materials.[14,52–54] Our systematic study provides the way to rapidly identify the $\theta_t$ using Raman spectroscopy in a twisted 3LG system, contributing to the development of twistronics.

See the supplementary material for fabrication details, Raman spectra of our multiple samples in a wider Raman shift range (showing the change of R and R′ peak position and the 2D peak intensity as a function of $\theta_t$), the 2D peak position of natural ABA and the artificial non-twisted 3LG on $SiO_2$ and hBN, and the ABC-like 2D peak spectra of NT2.

## AUTHORS' CONTRIBUTIONS

All authors have given approval to the final version of the manuscript. S.K. and D.L. contributed equally to this work.

This work was supported by the POSCO Science Fellowship of POSCO TJ Park Foundation, the National Research Foundation of Korea (NRF) grant funded by the Korean government (MSIT) (No. NRF-2020R1A4A1019266), and Nano-Material Technology Development program (No. NRF-2016M3A7B4909942) through the NRF, funded by the Ministry of Science and ICT, Korea. S. Yu and J. Fan were supported by the Air Force Office of Scientific Research (AFOSR) Multidisciplinary University Research Initiative (MURI) under Award No. FA9550-16-1-0031. We also thank Kyounghwan Kim for discussions.

## DATA AVAILABILITY

The data that support the findings of this study are available within the article and its supplementary material. Additional raw data are available from the corresponding author upon reasonable request.

## REFERENCES

[1]E. Koren, I. Leven, E. Lörtscher, A. Knoll, O. Hod, and U. Duerig, Nat. Nanotechnol. **11**, 752 (2016).
[2]Y. Cao, J. Y. Luo, V. Fatemi, S. Fang, J. D. Sanchez-Yamagishi, K. Watanabe, T. Taniguchi, E. Kaxiras, and P. Jarillo-Herrero, Phys. Rev. Lett. **117**, 116804 (2016).
[3]E. M. Alexeev, D. A. Ruiz-Tijerina, M. Danovich, M. J. Hamer, D. J. Terry, P. K. Nayak, S. Ahn, S. Pak, J. Lee, J. I. Sohn, M. R. Molas, M. Koperski, K. Watanabe, T. Taniguchi, K. S. Novoselov, R. V. Gorbachev, H. S. Shin, V. I. Fal'ko, and A. I. Tartakovskii, Nature **567**, 81 (2019).
[4]J. C. W. Song and N. M. Gabor, Nat. Nanotechnol. **13**, 986 (2018).
[5]Y. Tang, L. Li, T. Li, Y. Xu, S. Liu, K. Barmak, K. Watanabe, T. Taniguchi, A. H. MacDonald, J. Shan, and K. F. Mak, Nature **579**, 353 (2020).
[6]Y. Cao, V. Fatemi, A. Demir, S. Fang, S. L. Tomarken, J. Y. Luo, J. D. Sanchez-Yamagishi, K. Watanabe, T. Taniguchi, E. Kaxiras, R. C. Ashoori, and P. Jarillo-Herrero, Nature **556**, 80 (2018).
[7]Y. Cao, V. Fatemi, S. Fang, K. Watanabe, T. Taniguchi, E. Kaxiras, and P. Jarillo-Herrero, Nature **556**, 43 (2018).
[8]G. Chen, A. L. Sharpe, P. Gallagher, I. T. Rosen, E. J. Fox, L. Jiang, B. Lyu, H. Li, K. Watanabe, T. Taniguchi, J. Jung, Z. Shi, D. Goldhaber-Gordon, Y. Zhang, and F. Wang, Nature **572**, 215 (2019).
[9]G. Chen, L. Jiang, S. Wu, B. Lyu, H. Li, B. L. Chittari, K. Watanabe, T. Taniguchi, Z. Shi, J. Jung, Y. Zhang, and F. Wang, Nat. Phys. **15**, 237 (2019).
[10]X. Liu, Z. Hao, E. Khalaf, J. Y. Lee, Y. Ronen, H. Yoo, D. Haei Najafabadi, K. Watanabe, T. Taniguchi, A. Vishwanath, and P. Kim, Nature **583**, 221 (2020).
[11]C. Shen, Y. Chu, Q. Wu, N. Li, S. Wang, Y. Zhao, J. Tang, J. Liu, J. Tian, K. Watanabe, T. Taniguchi, R. Yang, Z. Y. Meng, D. Shi, O. V. Yazyev, and G. Zhang, Nat. Phys. **16**, 520 (2020).
[12]Y. Shi, S. Xu, M. M. A. Ezzi, N. Balakrishnan, A. Garcia, B. Tsim, C. Mullan, J. Barrier, N. Xin, B. A. Piot, T. Taniguchi, K. Watanabe, A. Carvalho, A. Mishchenko, A. K. Geim, V. I. Fal'ko, S. Adam, A. H. C. Neto, and K. S. Novoselov, arXiv:2004.12414 (2020).
[13]S. Chen, M. He, Y. H. Zhang, V. Hsieh, Z. Fei, K. Watanabe, T. Taniguchi, D. H. Cobden, X. Xu, C. R. Dean, and M. Yankowitz, Nat. Phys. **17**, 374–380 (2021).
[14]A. C. Ferrari and D. M. Basko, Nat. Nanotechnol. **8**, 235 (2013).
[15]L. M. Malard, M. A. Pimenta, G. Dresselhaus, and M. S. Dresselhaus, Phys. Rep. **473**, 51 (2009).
[16]M. A. Pimenta, G. Dresselhaus, M. S. Dresselhaus, L. G. Cançado, A. Jorio, and R. Saito, Phys. Chem. Chem. Phys. **9**, 1276 (2007).
[17]C. Stampfer, F. Molitor, D. Graf, K. Ensslin, A. Jungen, C. Hierold, and L. Wirtz, Appl. Phys. Lett. **91**, 241907 (2007).
[18]S. Pisana, M. Lazzeri, C. Casiraghi, K. S. Novoselov, A. K. Geim, A. C. Ferrari, and F. Mauri, Nat. Mater. **6**, 198 (2007).
[19]C. Neumann, S. Reichardt, P. Venezuela, M. Drögeler, L. Banszerus, M. Schmitz, K. Watanabe, T. Taniguchi, F. Mauri, B. Beschoten, S. V. Rotkin, and C. Stampfer, Nat. Commun. **6**, 8429 (2015).
[20]D. Yoon, Y. W. Son, and H. Cheong, Phys. Rev. Lett. **106**, 155502 (2011).
[21]M. Huang, H. Yan, T. F. Heinz, and J. Hone, Nano Lett. **10**, 4074 (2010).
[22]A. C. Ferrari, J. C. Meyer, V. Scardaci, C. Casiraghi, M. Lazzeri, F. Mauri, S. Piscanec, D. Jiang, K. S. Novoselov, S. Roth, and A. K. Geim, Phys. Rev. Lett. **97**, 187401 (2006).
[23]D. Graf, F. Molitor, K. Ensslin, C. Stampfer, A. Jungen, C. Hierold, and L. Wirtz, Nano Lett. **7**, 238 (2007).
[24]V. Carozo, C. M. Almeida, E. H. M. Ferreira, L. G. Cançado, C. A. Achete, and A. Jorio, Nano Lett. **11**, 4527 (2011).
[25]K. Kim, S. Coh, L. Z. Tan, W. Regan, J. M. Yuk, E. Chatterjee, M. F. Crommie, M. L. Cohen, S. G. Louie, and A. Zettl, Phys. Rev. Lett. **108**, 246103 (2012).
[26]V. Carozo, C. M. Almeida, B. Fragneaud, P. M. Bedê, M. V. O. Moutinho, J. Ribeiro-Soares, N. F. Andrade, A. G. Souza Filho, M. J. S. Matos, B. Wang, M. Terrones, R. B. Capaz, A. Jorio, C. A. Achete, and L. G. Cançado, Phys. Rev. B **88**, 085401 (2013).
[27]J. B. Wu, X. Zhang, M. Ijäs, W. P. Han, X. F. Qiao, X. L. Li, D. S. Jiang, A. C. Ferrari, and P. H. Tan, Nat. Commun. **5**, 5309 (2014).
[28]K. Kim, M. Yankowitz, B. Fallahazad, S. Kang, H. C. P. Movva, S. Huang, S. Larentis, C. M. Corbet, T. Taniguchi, K. Watanabe, S. K. Banerjee, B. J. LeRoy, and E. Tutuc, Nano Lett. **16**, 1989 (2016).

[29]L. A. Ponomarenko, R. V. Gorbachev, G. L. Yu, D. C. Elias, R. Jalil, A. A. Patel, A. Mishchenko, A. S. Mayorov, C. R. Woods, J. R. Wallbank, M. Mucha-Kruczynski, B. A. Piot, M. Potemski, I. V. Grigorieva, K. S. Novoselov, F. Guinea, V. I. Fal'ko, and A. K. Geim, Nature **497**, 594 (2013).
[30]C. Cong, T. Yu, K. Sato, J. Shang, R. Saito, G. F. Dresselhaus, and M. S. Dresselhaus, ACS Nano **5**, 8760 (2011).
[31]C. H. Lui, Z. Li, Z. Chen, P. V. Klimov, L. E. Brus, and T. F. Heinz, Nano Lett. **11**, 164 (2011).
[32]H. Zhao, Y. C. Lin, C. H. Yeh, H. Tian, Y. C. Chen, D. Xie, Y. Yang, K. Suenaga, T. L. Ren, and P. W. Chiu, ACS Nano **8**, 10766 (2014).
[33]J. M. B. Lopes dos Santos, N. M. R. Peres, and A. H. Castro Neto, Phys. Rev. Lett. **99**, 256802 (2007).
[34]E. McCann and V. I. Fal'ko, Phys. Rev. Lett. **96**, 086805 (2006).
[35]K. S. Novoselov, Z. Jiang, Y. Zhang, S. V. Morozov, H. L. Stormer, U. Zeitler, J. C. Maan, G. S. Boebinger, P. Kim, and A. K. Geim, Science **315**, 1379 (2007).
[36]S. Reich, J. Maultzsch, C. Thomsen, and P. Ordejón, Phys. Rev. B **66**, 035412 (2002).
[37]Z. Ni, Y. Wang, T. Yu, Y. You, and Z. Shen, Phys. Rev. B **77**, 235403 (2008).
[38]L. M. Malard, M. H. D. Guimarães, D. L. Mafra, M. S. C. Mazzoni, and A. Jorio, Phys. Rev. B **79**, 125426 (2009).
[39]J. C. Charlier, X. Gonze, and J. P. Michenaud, Carbon **32**, 289 (1994).
[40]F. Forster, A. Molina-Sanchez, S. Engels, A. Epping, K. Watanabe, T. Taniguchi, L. Wirtz, and C. Stampfer, Phys. Rev. B **88**, 085419 (2013).
[41]L. Wang, Z. Chen, C. R. Dean, T. Taniguchi, K. Watanabe, L. E. Brus, and J. Hone, ACS Nano **6**, 9314 (2012).
[42]H. Yoo, R. Engelke, S. Carr, S. Fang, K. Zhang, P. Cazeaux, S. H. Sung, R. Hovden, A. W. Tsen, T. Taniguchi, K. Watanabe, G. C. Yi, M. Kim, M. Luskin, E. B. Tadmor, E. Kaxiras, and P. Kim, Nat. Mater. **18**, 448 (2019).
[43]A. Kerelsky, C. Rubio-Verdú, L. Xian, D. M. Kennes, D. Halbertal, N. Finney, L. Song, S. Turkel, L. Wang, K. Watanabe, T. Taniguchi, J. Hone, C. Dean, D. Basov, A. Rubio, and A. N. Pasupathy, arXiv:1911.00007 (2019).
[44]H. Li, M. I. B. Utama, S. Wang, W. Zhao, S. Zhao, X. Xiao, Y. Jiang, L. Jiang, T. Taniguchi, K. Watanabe, A. Weber-Bargioni, A. Zettl, and F. Wang, Nano Lett. **20**, 3106 (2020).
[45]M. Zhu, D. Ghazaryan, S. K. Son, C. R. Woods, A. Misra, L. He, T. Taniguchi, K. Watanabe, K. S. Novoselov, and Y. Cao, 2D Mater. **4**, 011013 (2016).
[46]S. Carr, D. Massatt, S. Fang, P. Cazeaux, M. Luskin, and E. Kaxiras, Phys. Rev. B **95**, 075420 (2017).
[47]E. Y. Andrei and A. H. MacDonald, Nat. Mater. **19**, 1265 (2020).
[48]K. Kim, A. DaSilva, S. Huang, B. Fallahazad, S. Larentis, T. Taniguchi, K. Watanabe, B. J. LeRoy, A. H. MacDonald, and E. Tutuc, Proc. Natl. Acad. Sci. U. S. A. **114**, 3364 (2017).
[49]M. Lamparski, B. Van Troeye, and V. Meunier, 2D Mater. **7**, 025050 (2020).
[50]I. Brihuega, P. Mallet, H. González-Herrero, G. Trambly de Laissardière, M. M. Ugeda, L. Magaud, J. M. Gómez-Rodríguez, F. Ynduráin, and J. Y. Veuillen, Phys. Rev. Lett. **109**, 196802 (2012).
[51]A. Kerelsky, L. J. McGilly, D. M. Kennes, L. Xian, M. Yankowitz, S. Chen, K. Watanabe, T. Taniguchi, J. Hone, C. Dean, A. Rubio, and A. N. Pasupathy, Nature **572**, 95 (2019).
[52]M. S. Dresselhaus, A. Jorio, M. Hofmann, G. Dresselhaus, and R. Saito, Nano Lett. **10**, 751 (2010).
[53]N. Sheremetyeva, M. Lamparski, C. Daniels, B. Van Troeye, and V. Meunier, Carbon **169**, 455 (2020).
[54]J.-B. Wu, M.-L. Lin, X. Cong, H.-N. Liu, and P.-H. Tan, Chem. Soc. Rev. **47**, 1822 (2018).